

Dissolution, Agglomerate Morphology, and Stability Limits of Protein-Coated Silver Nanoparticles

Matthew N. Martin,^{*,†,‡,⊥} Andrew J. Allen,[†] Robert I. MacCuspie,[†] and Vincent A. Hackley[†]

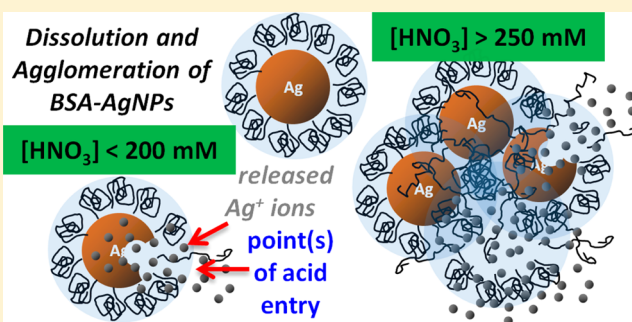
[†]Material Measurement Laboratory, National Institute of Standards and Technology, 100 Bureau Drive, Gaithersburg, Maryland 20899-8520, United States

[‡]Materials Science and Engineering Department, University of Maryland, College Park, Maryland 20742-2115, United States

[⊥]Department of Applied Mathematics and Sciences, Khalifa University, P.O. Box 127788, Abu Dhabi, UAE

S Supporting Information

ABSTRACT: Little is understood regarding the impact that molecular coatings have on nanoparticle dissolution kinetics and agglomerate formation in a dilute nanoparticle dispersion. Dissolution and agglomeration processes compete in removing isolated nanoparticles from the dispersion, making quantitative time-dependent measurements of the mechanisms of nanoparticle loss particularly challenging. In this article, we present in situ ultra-small-angle X-ray scattering (USAXS) results, simultaneously quantifying dissolution, agglomeration, and stability limits of silver nanoparticles (AgNPs) coated with bovine serum albumin (BSA) protein. When the BSA corona is disrupted, we find that the loss of silver from the nanoparticle core is well matched by a second-order kinetic rate reaction, arising from the oxidative dissolution of silver. Dissolution and agglomeration are quantified, and morphological transitions throughout the process are qualified. By probing the BSA-AgNP suspension around its stability limits, we provide insight into the destabilization mechanism by which individual particles rapidly dissolve as a whole rather than undergo slow dissolution from the aqueous interface inward, once the BSA layer is breached. Because USAXS rapidly measures over the entire nanometer to micrometer size range during the dissolution process, many insights are also gained into the stabilization of NPs by protein and its ability to protect the labile metal core from the solution environment by prohibiting the diffusion of reactive species. This approach can be extended to a wide variety of coating molecules and reactive metal nanoparticle systems to carefully survey their stability limits, revealing the likely mechanisms of coating breakdown and ensuing reactions.



INTRODUCTION

Silver nanoparticles (AgNPs) have received increasing attention due to their antimicrobial properties and incorporation into consumer products.^{1,2} Aqueous AgNPs are not stable; in natural water systems³ they dissolve into silver ions^{4–6} and sometimes reform^{7–9} if they are not sufficiently stabilized. Silver ions (Ag^+) can be toxic to human cells in high doses¹⁰ and may pose environmental health and safety risks,¹¹ or conversely, the natural antibacterial properties of Ag ions can be used, for example, to reduce the infection risk of wounds.¹² Typically, AgNPs oxidatively dissolve in water¹³ or form agglomerates due to changes in their colloidal stability resulting from interactions with ions (e.g., Na^+ and Cl^-)^{14–17} and sulfur-containing species.^{18,19} These processes occur simultaneously, and it can be challenging to distinguish between the loss of AgNPs due to dissolution or agglomeration (and thus sedimentation).^{14,20,21} Certainly, the end result is a net loss of Ag atoms from singly dispersed AgNPs and either a high concentration of Ag ions in solution or AgNPs trapped in agglomerates as sediment. These processes will dictate the eventual fate and availability of AgNPs and their transforma-

tional products. Because AgNPs with various coatings are used in many consumer products,²² it is critical to understand how the NP surface is destabilized and the subsequent dissolution process. However, many measurement methods fail to capture the competing destabilization processes, resulting in a knowledge gap surrounding the mechanisms of colloidal destabilization and exactly how a surface coating protects a particle against dissolution.

Several separation techniques, such as centrifugation, can be combined with methods that accurately measure total silver, for example, atomic absorption or inductively coupled plasma mass spectrometry (ICP-MS), to infer dissolved silver content.^{23,24} Analytical ultracentrifugation has been used to separate agglomerates²⁵ as well as to measure sedimentation.²⁶ Field flow fractionation has also been explored to separate agglomerates and provide size distributions and has been coupled to ICP-MS.²⁷ These methods are destructive or alter the initial dispersion, making it cumbersome to merge the

Received: August 7, 2014

Published: August 19, 2014

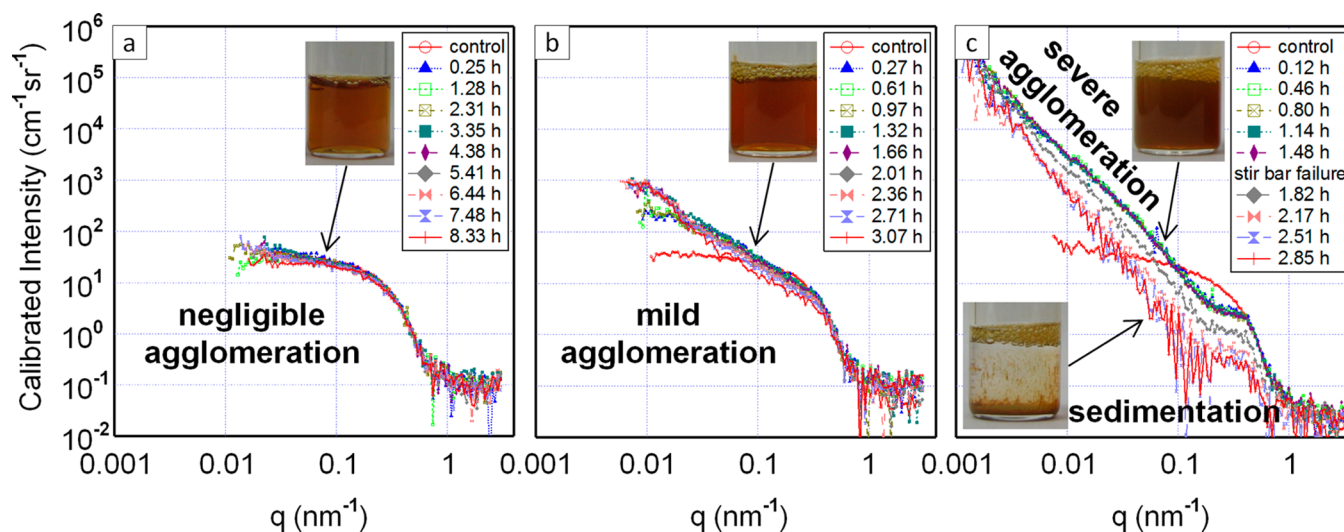


Figure 1. Stability regimes of BSA-AgNPs in HNO_3 measured by absolute-intensity-calibrated USAXS. (a) In 50 mM HNO_3 , BSA-AgNPs slowly dissolve with almost no agglomeration, as evidenced by the relatively flat, low- q scattering curve and optical clarity of the solution (inset). (b) In 250 mM HNO_3 , BSA-AgNPs simultaneously agglomerate and dissolve while the solution darkens. (c) In 500 mM HNO_3 , the BSA coating completely destabilizes, causing rapid clustering of principal particles into agglomerates, as seen in the large scattering intensities at low q values and the dark turbid suspension. In this case, “steady” dissolution proceeds as long as the particles are stirred; otherwise, they sediment, as detected by an exponential decay in the scattering intensity and by visual inspection.

techniques for time-resolved studies, although progress has been made by coupling these to nondestructive light-extinction (scattering + absorption) methods, such as ultraviolet–visible extinction spectroscopy (UV–vis)^{24,28,29} and dynamic light scattering (DLS).^{30,31} DLS is strongly biased toward small volume fractions of large agglomerates because the scattering intensity varies as the sixth power of the particle diameter d (i.e., d^6). For example, a single 150 nm agglomerate will scatter as much light as 10^6 singly dispersed 15 nm nanoparticles. Meanwhile, coupling between embedded NPs in an agglomerate alters the surface plasmon resonance of the nanoparticles and greatly complicates measurement by UV–vis. In general, it is difficult to quantify the destabilization of AgNPs because such quantification requires simultaneous measurements over time of the principal particles and agglomerate size distributions, together with their Ag absolute volume fractions (i.e., NP concentrations). Despite these challenges, it remains highly desirable to understand better how coating molecules stabilize the particle surface, how and under what conditions AgNPs dissolve or agglomerate, and how these processes compete.

Here, we employ in situ ultra-small-angle X-ray scattering (USAXS) to probe the competing dissolution and agglomeration processes for AgNPs protected by a highly stabilizing protein coating, bovine serum albumin (BSA), in extremely acidic environments. We push BSA to its stability limits in order to measure its impact on the dissolution kinetics and intermediate agglomerate morphologies formed during dissolution. BSA was chosen due to the biological relevance of albumin as the most abundant protein in mammalian blood plasma, its widespread use in biology and nanoparticle engineering,^{32–35} and its remarkable ability to buffer aqueous systems against harsh conditions.^{17,36,37} We have performed the dissolution experiments in nitric acid as a model system for Ag dissolution, bypassing the complications of Cl or S side reactions that would occur in hydrochloric or sulfuric acids or in synthetic stomach fluids.¹⁶ Because USAXS can concurrently measure the size distribution and concentration, quantification

of the AgNP and agglomerate morphology from the sub-10 nm to micrometer size scale is achievable throughout the entire reaction process. Our structural model accounts for dissolved silver from nanoparticles and agglomerates, and possible agglomerate growth mechanisms are discussed. We find a second-order reaction governing the loss of Ag from the nanoparticles and attribute this to oxidative dissolution, consistent with previous reports for milder reaction conditions.¹³ By simultaneously measuring dissolution and agglomeration, a model is presented that accurately distinguishes the entangled dissolution and agglomeration processes. To the best of our knowledge, this is the first quantitative study of the mechanisms of AgNP dissolution in a strongly agglomerating environment and one of the first studies to elucidate the stability limits of coating nanoparticles with protein. This method can be extended to analyzing the stability of other highly relevant coating molecules for AgNPs as well as other metal nanoparticles.

RESULTS AND DISCUSSION

Stability Limits of BSA-AgNPs. The colloidal stability limits for BSA-coated AgNPs can be evaluated by several different methods. Simple visual inspection can reveal the turbidity of a solution and provide a crude guide as to what is happening in solution. DLS and UV–vis can provide useful information about changes to the particle size distribution and plasmon peak shifts (Supporting Information, Figures S1 and S2, respectively); however, they cannot quantitatively determine detailed structure on the nanoscale, simply because the wavelength of visible light is too large. However, the wavelength of the X-rays used here ($\lambda = 0.073$ nm for 16.9 keV X-rays) is much smaller than the principal nanoparticles ($d \approx 10$ nm) measured, so it is possible to discern both nanoparticle and interparticle structure.

USAXS plots surveying the stability regimes of BSA-AgNPs in different concentrations of nitric acid are presented in Figure 1. Equal volumes of nitric acid solutions and aqueous BSA-AgNP dispersions (initial silver volume fractions: $\phi_{\text{Ag}} \approx 5 \times$

10^{-5}) were mixed, yielding varying effects based on the concentration of acid. In 50 mM HNO_3 (Figure 1a), BSA-AgNPs are fairly stable, and the scattering intensity $I(q)$ decays slowly with negligible amounts of agglomerates at low q , where

$$q = \frac{4\pi}{\lambda} \sin \theta \quad (1)$$

is the magnitude of the scattering vector and θ is half of the scattering angle. This stability is also confirmed by the relative optical clarity of the solution (Figure 1a inset), which resembles the control sample in the absence of HNO_3 . A threshold is observed near 50 mM HNO_3 , below which BSA protects very well, likely due to buffering of the acid and preservation of the nanoparticle surface.

In 250 mM HNO_3 (Figure 1b), particles begin to agglomerate, as can be seen in the increased scattering intensity sloping upward toward low q . The scattering associated with the principal nanoparticle population blends into that from the agglomerates. This suggests the formation of agglomerates in a size range from tens of nanometers to $\sim 1 \mu\text{m}$. The scattering intensity then decreases over time as particles dissolve (and agglomerates sediment).

In 500 mM HNO_3 (Figure 1c), there are many signatures in the USAXS data. Interestingly, the terminal slope at high q does not change; however, a large shoulder forms between $q \approx 0.2$ and 0.4 nm^{-1} . This indicates a clustering of principal particles at a characteristic distance of $2\pi/q$ from one another (here 10 to 20 nm), creating a structural level that can be modeled as particles interfering with the scattering of their nearest neighbors. We account for this scattering by using the model depicted in Figure 2. The shoulder rises steeply into rapid agglomeration, as evinced at low q . The overall scattering intensity decayed predictably with time, after the addition of

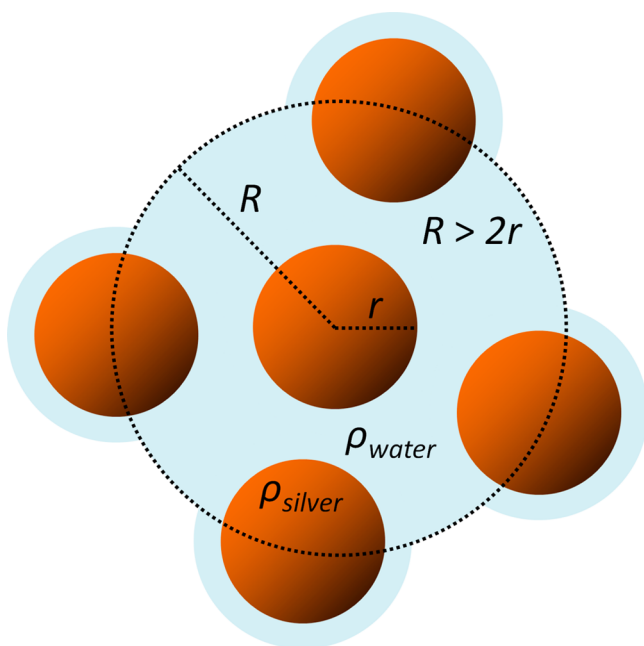


Figure 2. Schematic of the model used to fit USAXS data during the dissolution process. Individual AgNPs are modeled as spheres with scattering length density ρ_{silver} immersed in water, ρ_{water} . A structure factor incorporating NP packing fraction and average interparticle center-to-center distance, R , quantifies the particle–particle correlations within the closely packed NP clusters (i.e., agglomerates).

acid, until the stir bar failed between 1.48 and 1.82 h. Sedimentation then became dominant, with a corresponding exponential decay in the scattering intensity with time.^{38–40}

The colloidal stability of the BSA-coated AgNPs is directly related to the charge structure and pH stability of the BSA coating. The isoelectric point of free BSA has been reported between pH 4.8 and 5.6,^{36,41–43} implying that BSA is charge neutral near pH 5. A change in solution pH below 5 causes the stable tertiary heart-shaped BSA structure to elongate, often called the N–F transition (normal-fast).⁴⁴ Below pH 2.5, free BSA breaks down and elongates further (the E-form or expanded form), and when on the surface of a nanoparticle (bound BSA), the transition pH can be lowered.⁴³ The measurement of pH for a dissolving Ag system can be experimentally difficult due to the contamination of electrodes by deposited Ag. Therefore, we have not systematically measured the pH as a function of time for the various acid cases.

However, we did find results that agree with the above predictions (Supporting Information, Table S1). On the basis of pH measurements at lower BSA-AgNP concentrations, for the 500 mM HNO_3 case we estimate the pH to be ~ 1.9 , which is well below the N–F transition (pH ~ 5) and just below the F–E transition (pH 2.5). Previous DLS studies on dilute dispersions of 60 nm gold nanoparticles coated with BSA⁴³ suggest that there is a significant and predictable change in the BSA coating thickness ($\sim 4 \text{ nm}$) near pH 2.7, where the BSA lengthens and opens up spots on the nanoparticle surface, but above this pH value, the hydrodynamic diameter (NP core + BSA corona) remains constant. This could explain why we see rapid dissolution in the strong acid cases (i.e., 500 and 375 mM) and strong protection in the weak acid cases (i.e., 50 mM). Thus, it is understandable that BSA coatings break down in 500 mM HNO_3 as BSA elongates on the NP surface, exposing holes in the protective coating and potential paths for acid to reach the Ag core and hence AgNP dissolution. Clearly, the nature of BSA and its role in protecting AgNPs from acid dissolution are complex, but we have sought to develop a model for quantifying the actual molar amount of Ag in nanoparticle form in a dissolving and agglomerating BSA-AgNP dispersion.

USAXS Model. To separate and quantify the loss of silver in the agglomerating and dissolving BSA-AgNPs system, we analyze the scattering intensity $I(q)$ from dispersed particles of radius r as well as the structure formed by particles in close proximity

$$I(q) = \phi |\Delta\rho|^2 v_p F^2(q, r) S(q, R) \quad (2)$$

where ϕ is the nanoparticle volume fraction, v_p is the single-particle volume, and $|\Delta\rho|^2$ is the scattering contrast between the scattering particle and the matrix (i.e., the acidic aqueous suspension medium). $F(q, r)$ is the geometrical form factor for spheres

$$F(q, r) = 3 \frac{\sin(qr) - qr \cos(qr)}{(qr)^3} \quad (3)$$

and $S(q, R)$ is an approximate structure factor associated with the packing of multiple particles in close proximity.⁴⁵

$$S(q, R) = \frac{1}{1 + 8\phi_{\text{loc}} F(q, R)}$$

$$= \frac{1}{1 + 8\phi_{\text{loc}} \left| 3 \frac{\sin(qR) - qR \cos(qR)}{(qR)^3} \right|} \quad (4)$$

Here, the packing fraction ϕ_{loc} is the ratio of the occupied to available volume formed by a sphere with radius R centered on a particle. Thus, R can be viewed as the average nearest-neighbor center-to-center distance with particle/local volume ϕ_{loc} . Restated, this structure factor signifies the packing of spheres into a volume. The schematic of this model can be seen in Figure 2. Simple limiting checks can be made on the model; by letting $\phi_{\text{loc}} = 0$ or $R \rightarrow \infty$, one can see $S(q, R) \rightarrow 1$ and we recover the scattering from singly dispersed spheres. When $\phi_{\text{loc}} \approx 0.74$ and $R = 2r$, one obtains the maximal physically allowed volume fraction for a uniform distribution of spheres^{45,46} with particle surfaces touching, corresponding to face-centered cubic or hexagonal close packing. Disordered, glassy, or random orientations would show lower values of ϕ_{loc} .

For the agglomerates, we use a spherical model (eq 3). Then, apparent volume fractions are adjusted after modeling to account for the Ag-occupied and available space in the close pack according to

$$\phi_{\text{Ag, agglomerate}} = \phi_{\text{loc}} \left(\phi_{\text{Ag, apparent, agglomerate}} \frac{|\Delta\rho|^2}{|\Delta\rho|_{\text{pack}}^2} \right) \quad (5)$$

in which $|\Delta\rho|^2 = |\rho_{\text{Ag}} - \rho_{\text{water}}|^2$, and the reduced scattering contrast in the close pack is given by

$$|\Delta\rho|_{\text{pack}}^2 = |\phi_{\text{loc}} \rho_{\text{Ag}} - \rho_{\text{water}}|^2 \quad (6)$$

In summary, we are modeling the dissolving/agglomerating system with two size scales: principal particles having structural morphology similar to that of packed spheres and loose agglomerates with reduced volume fractions using packing fraction ϕ_{loc} . Because the actual system contains polydisperse spheres, the overall scattering intensity is a weighted sum of the nanoparticle size distribution (assumed to be a log-normal function) and eq 2 (the scattering for a given particle of size r), provided the system satisfies the dilute condition $\phi \approx \phi(1 - \phi)$. The present experiments used AgNPs of concentration $\phi < 10^{-4}$, so this condition is well met.

Volume Fraction and Diameter Results from Model Fitting. It is important to distinguish among several different physical processes occurring simultaneously, such as dissolution, agglomeration/clustering, and sedimentation. Because there is significant agglomeration in our system when the nitric acid concentration is high (i.e., $[\text{HNO}_3] \geq 250$ mM), AgNPs sediment. To extract dissolution and agglomeration kinetics from the sedimenting system, a magnetic stir bar was used in the sample reservoir. Figures 1 and 3 show dissolution for the 500 mM case until the stir bar failed, upon which there was an exponential drop in scattering (Figure 1) due to the loss of the NP volume fraction within the total sampled volume (Figure 3). (We have also added additional results to Figure 3 for 500 mM HNO_3 dissolution from a separate run with a non-sedimenting sample; for separate analysis of this sample, see the Supporting Information.) In each case when acid was added to the solution, loss of the overall Ag volume fraction immediately commenced. In 500 and 375 mM HNO_3 , there was a sudden drop in volume fraction due to rapid agglomeration, and then

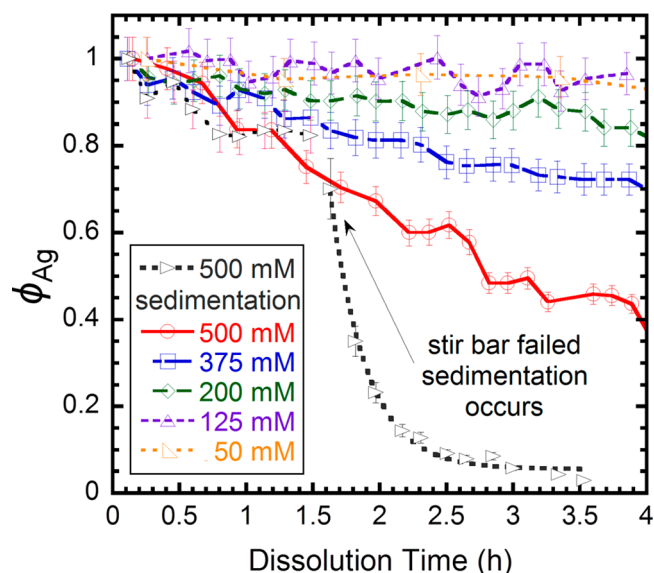


Figure 3. Silver volume fractions vs time during the dissolution of BSA-AgNPs in varying concentrations of HNO_3 . The volume fractions measured, ϕ_{Ag} , correspond to total silver (normalized to 1 for the initial condition) remaining in both singly dispersed principal particles and in particles within agglomerates. Each vertical bar represents an estimated 5% standard deviation uncertainty for each data point.

dissolution proceeded. The AgNP volume fraction was reduced from that measured immediately after the addition of acid, by ~ 18 and $\sim 14\%$ in the first 1.5 h, in 500 and 375 mM HNO_3 , respectively. Reaction in 200 mM HNO_3 caused only slight agglomeration, although the AgNP volume fraction was still reduced by 10% over the first 1.5 h. For 125 and 50 mM HNO_3 , negligible agglomeration occurred, and particles lost silver by dissolution at a constant rate that can be well fit by a straight line. The volume fraction loss rate together with the fit standard deviation uncertainties was determined to be 1.4 ± 0.5 and 1.4 ± 0.2 h^{-1} for 125 and 50 mM HNO_3 , respectively. Within these fit uncertainties, there is no evidence of any acid or particle concentration dependence, which indicates that the particles followed a zeroth-order reaction process with respect to HNO_3 at 125 and 50 mM concentrations. These results agree with the stability thresholds of BSA-AgNPs established above.

Presumably, the BSA-AgNP dispersion is stabilized by electrostatic and steric repulsion (from surface charge and the BSA), countering a van der Waals attraction between the metal cores. Thus, if the surfaces are neutralized and enough BSA is displaced, then particles will agglomerate because the repulsive force will vanish. Concentrations of $\text{HNO}_3 \geq 375$ mM seemingly disrupt the BSA coating, causing rapid agglomeration and unwinding of the BSA protein on the particle surface. This permits acid and oxygen access to the AgNP core, initiating oxidative dissolution very quickly. A concentration of 250 mM HNO_3 causes mild agglomeration, which can be attributed to the partial disruption of BSA surfaces. Below 250 mM HNO_3 , insufficient acid (i.e., protons) is added to destabilize the surface or cause BSA charge neutralization and coagulation. It is likely that single adsorbed BSA molecules are unraveled due to statistical concentration fluctuations of acid near the NP-solution interface; it is possible that either acidic gradients due to diffusion or patchy BSA coverage is responsible for the

dissolution losses. In practice, it is impossible to tell with USAXS which process truly occurs because we measure the sum of scattering from $\sim 10^{14}$ particles. However, the particle volume fraction still declines at a slow rate even at low acid concentrations. This leads us to believe that the particles are dissolved by the acid on an individual basis rather than by the simultaneous etching of all particles and that a loss in volume fraction is in fact a surface destabilization followed by rapid and complete whole particle dissolution. To confirm this scenario, it is useful to compare any variation in the diameter of the principal AgNPs in tandem with the volume fraction loss.

Figure 4 shows results quantifying the diameter change over time for both principal particles and agglomerates. Because of

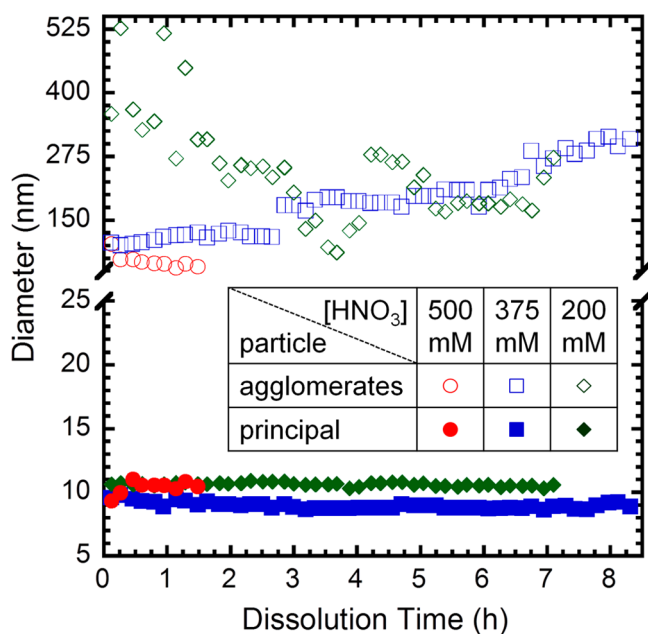


Figure 4. Mode diameter of principal BSA-AgNPs and median diameter of agglomerates vs time in varying concentrations of HNO₃. Principal particles do not change in diameter significantly and have tight size distributions, suggesting that dissolution does not grow or shrink the particle size universally. Agglomerates are large, growing between 50 and 600 nm with very broad size distributions.

the narrow width of the principal particle size distributions, the mode diameter, defined as the particle diameter associated with the maximum in the size distribution, was used to characterize the population. For principal BSA-AgNPs, the results are significant; in all cases, the mode diameters did not decrease or increase by any considerable amount. The 500 mM case changed by $-0.5 \pm 0.4 \text{ nm h}^{-1}$, and each of the others (375, 200, 125, and 50 mM HNO₃) changed in size by less than $0.10 \pm 0.03 \text{ nm h}^{-1}$. These results compare with an initial AgNP mode diameter of $\sim 10 \text{ nm}$. Stated simply, within the experimental uncertainties, principal particles are not significantly changing diameter during the dissolution process.

Because of the large variation in the width of the agglomerate size distributions produced, the mode and mean diameters extracted from a log-normal distribution are less representative of a nominal agglomerate size than the median diameter. Therefore, we have used the median diameter to characterize the agglomerate sizes. The median diameters of the agglomerates range between 50 and 600 nm. In 500 mM HNO₃, agglomerates initially form at $\sim 100 \text{ nm}$ and decrease to

$\sim 75 \text{ nm}$ in the first 0.5 h. Agglomerates then slowly continue to change in size by $-12 \pm 3 \text{ nm h}^{-1}$ to $\sim 60 \text{ nm}$, at which point it seems that the agglomerate diameter begins to stabilize. This rapid initial coagulation and then shrinking of the agglomerates indicates that Ag is being dissolved from the exterior of a BSA-AgNP agglomerate cluster until it reaches $\sim 60 \text{ nm}$ (four-particle-thick agglomerates). At this point (after $\sim 1.5 \text{ h}$), the stir bar failure and sedimentation artificially increase the measured median size progressively to well over $1 \mu\text{m}$ (data not shown for clarity). Fully dense silver particles of 60 to 100 nm diameter will sediment, while the large micrometer-scale agglomerates may be sufficiently loosely packed to remain as buoyant fractal clusters of BSA with embedded AgNPs (vide infra). The formation of fractal agglomerates at later dissolution times is confirmed when the slope of $I(q)$ at low q becomes linear in a log-log plot over several decades in q (Supporting Information). At this point, the agglomerate model discussed here becomes inapplicable, but fractal agglomeration is discussed in more detail later.

In 375 mM HNO₃, agglomerates initially formed with median diameters of just over $\sim 100 \text{ nm}$, similar to those in 500 mM HNO₃; however, in the 375 mM HNO₃ case, they grew at a rate of $25 \pm 1 \text{ nm h}^{-1}$ for more than 8 h. This is in contrast to the higher acid concentration and shows that agglomeration outperformed dissolution from the exterior of the BSA-AgNP agglomerates. There is a jump in the measured median diameter because this is where the agglomerates begin to exhibit power-law scaling over the remaining q range, and our spherical agglomerate model becomes much less reliable. Eventually, however, the agglomerates stop growing, and dissolution begins to take over, ultimately depleting the AgNPs from the dispersion (seen by eye after $\sim 16 \text{ h}$). The complexities of the 375 mM HNO₃ case are discussed in detail later.

In 200 mM HNO₃, the agglomerate volume fraction is so low (initially $<1\%$ of the total AgNP volume fraction) that only small amounts of large agglomerates 300 to 550 nm in size are detected. However, as dissolution proceeds, the agglomerate population that survives accounts for $\sim 2.7\%$ of the total AgNP volume fraction and the agglomerate diameter fluctuates between 100 and 300 nm. This remains a very weak agglomerate component, and the statistical fluctuations in the fitted agglomerate diameter are essentially artifacts of the model fits. In 125 and 50 mM HNO₃, there is so little agglomerate volume fraction that the initial agglomerates seem to be $\sim 300 \text{ nm}$, similar to the 200 mM case, although the data are so noisy and weak that the least-squares fit uncertainty is greater than the predicted diameter change. In fact, in 50 mM HNO₃, agglomerates are not detectable at all for the first 1.5 h.

Morphological Transitions during Agglomeration.

When AgNPs rapidly agglomerate, such as in 500 and 375 mM HNO₃, similar processes ensue, possessing slightly different clustering dynamics. The approximate packing fraction ϕ_{loc} derived from our model for the interference scattering between closely neighboring AgNPs, can be monitored to get an estimate of the effective BSA-AgNP density within a cluster. When particles agglomerate, the kinetic process is called random packing or jamming, corresponding to slightly different clustering dynamics.⁴⁷ In reality, the AgNP dispersions contain a polydisperse distribution of principal particles, which can cause the packing fractions to deviate from those found in the theoretical literature. On addition of 500 mM HNO₃, the packing fraction immediately takes a value of 0.54, very close to

that of random loosely packed clusters.^{48,49} The distance between particle surfaces in the model (the amount by which the modeled particle nearest-neighbor center-to-center distance exceeds the particle diameter, i.e., $R - 2r$) is between 3 and 5 nm, which could be accounted for by the presence of a BSA coating between neighboring particles. We naturally expect AgNPs in 500 mM HNO₃ to form loosely jammed agglomerates because of the rapid AgNP clustering that occurs at high acid concentrations. Thus, it becomes interesting to compare this agglomerating packing fraction with that found at lower acid concentrations.

In 375 mM HNO₃, the packing fraction and center-to-center distance are plotted versus time in Figure 5. The initial packing fraction is 0.64, which is very close to the case of random close packing^{47,48} or a “maximally random jammed” phase.⁵⁰ Over 8 h, the packing fraction decreases to 0.43, below that of random loose packing. This change occurs fairly linearly in time, most likely indicating that particles are dissolving inside the close pack. Additionally, the center-to-center nearest-neighbor distance is gradually increasing with time, suggesting that the AgNPs are loosening within the agglomerates. The predictable growth of the power-law scattering with time to lower q values most likely signals the growth of fractal agglomerates, which as highly branched structures can possess packing fractions different from random loose packing. Across samples, we consistently measure power-law scalings in scattering intensity between 2.4 and 2.6 at low q , which is consistent with a diffusion-limited aggregation scenario⁵¹ (power-law fitting results in the Supporting Information). Nam et al. reported agglomerated 12 nm silica particles with fractal dimensions of 2.57 in aerated solutions.⁵² In both 500 and 375 mM HNO₃, there is a “loosening” of the agglomerates in terms of the occupied Ag fractions. In the 500 mM case, this manifests itself by a significant change in the interparticle distance, whereas the 375 mM case shows a decrease in the packing fraction. In both cases, there is a decrease in Ag within the initial close-packed clusters, suggesting that dissolution is continuously processing the agglomerates.

Ag⁺ Release from the Nanoparticle Surface. The total Ag dissolved from nanoparticle form is essentially described by the volume fraction versus dissolution time plots in Figure 3. However, to obtain a complete picture of what is happening in the suspension, we must look at the reactions of the total dissolving system. There are many competing effects: BSA destabilization, agglomeration, oxidative dissolution, and even dynamic particle processing.⁷ At low acid concentrations where the BSA coating protects the Ag core well ($[\text{HNO}_3] < 200$ mM), the silver volume fraction loss is best described by a zeroth-order reaction rate with respect to HNO₃. At higher acid concentrations where there is significant disruption of the BSA coating, we see a loss of Ag from the nanoparticle form that is not quite linear with time. Plotting the inverse volume fraction versus time reveals the best linear fits for acid concentrations >250 mM, corresponding to a second-order rate with respect to the formation of Ag⁺, as shown in Figure 6.

Plotting the inverse volume fraction, $1/\phi_{\text{Ag}}$, relative to the initial value after the addition of acid reveals a linear relationship that is representative of a second-order rate reaction. We infer from this that among all competing processes, the breakdown of nanoparticulate Ag is dominated by oxidative dissolution:

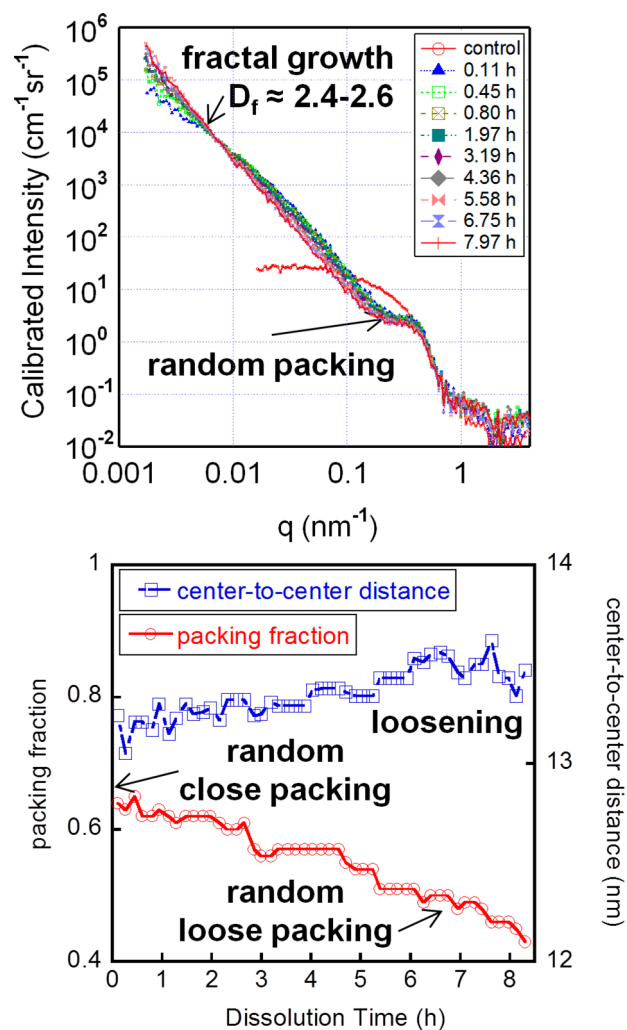
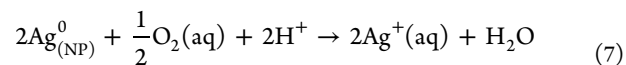


Figure 5. Scattering curves (top panel) and structure factor parameters (bottom panel) during dissolution over 8 h. Over time, particles move through solution and stick to growing agglomerate clusters, giving rise to a power-law slope with values between 2.4 and 2.6 at low q , which is well described by 3D diffusion-limited aggregation fractals. In 375 mM HNO₃, principal particles initially cluster, forming a random close pack with an average ~ 13.2 nm center-to-center distance between neighboring AgNPs. Over 8 h, the packing fraction decreases to values closer to a random loose pack with a 13.4 nm average center-to-center distance between neighboring AgNPs of average diameter 9.0 nm. This suggests a 4.4 nm average distance between neighboring AgNP surfaces, which can be directly explained by the presence of a BSA coating. The loosening could arise from the breakup of agglomerates or, more likely, the dissolution of localized AgNPs in the packed structure.



This scenario has been proposed for a citrate-stabilized AgNP system dissolving in dilute acid systems.⁵ Clearly, another large contributor to the reaction is the nitric acid itself. Both dissolved oxygen and HNO₃ will oxidize the Ag, which results in an increased production of silver ions in solution predominantly through proton-promoted dissolution of the oxidized surface. It is known that the AgNP surface hosts many complex chemical processes affecting Ag⁺ release that occur simultaneously: stabilization by sulfidation, dissolution by oxidation, protection by ligand adsorption (BSA), and natural

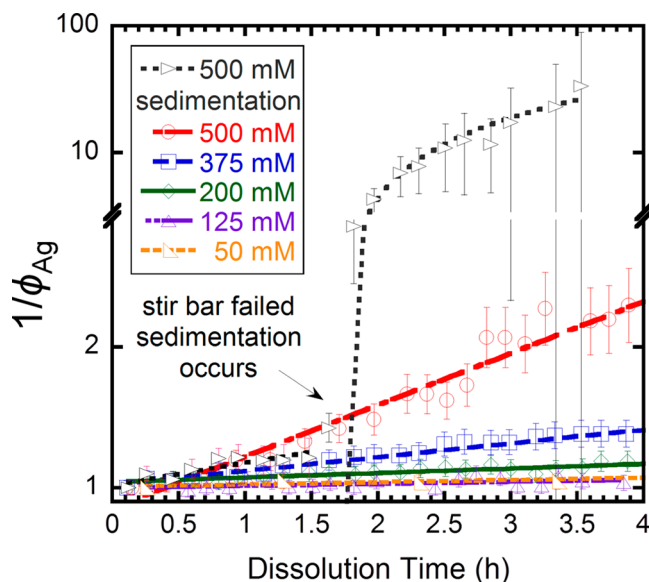


Figure 6. Loss of nanoparticulate silver can be seen as a second-order process. Below 200 mM HNO_3 , the intact BSA corona strongly inhibits the reaction with the Ag core, and dissolution is independent of acid concentration (zeroth order). However, once the concentration barrier is overcome and the BSA layer is disrupted above 200 mM HNO_3 , the rate-limiting reaction is suspected to be the oxidative dissolution of neutral AgNPs (second order), corresponding to the reaction $2\text{Ag}_{(\text{NP})}^0 + \frac{1}{2}\text{O}_2(\text{aq}) + 2\text{H}^+ \rightarrow 2\text{Ag}^+(\text{aq}) + \text{H}_2\text{O}$. Lines are least-squares fits to the data, and uncertainties were propagated from volume fraction measurements by the method of partial derivatives. This confirms that we can measure dissolution quite well, but sedimentation wipes out the volume fraction so efficiently that it is difficult to measure after several hours, as indicated by the increasingly larger uncertainties at later dissolution times.

organic matter as well as ion exchange.¹³ Here we provide strong evidence that the dissolution process for BSA-AgNPs is mechanistically driven by BSA coating breakdown and most likely followed by oxidative dissolution. Typically, zeroth-order reactions exist when reactants saturate a surface or cannot overcome a concentration barrier to initiate a reaction; thus it is logical for low acid concentrations, where BSA does not completely break down, that the dissolution rate will be independent of the acid concentration. However, once the silver core is accessible, nothing prevents the oxidative dissolution of the AgNP. In other words, a stable coating of BSA shields (buffers) the reactive metal core from oxygen and acid in the solution environment.⁵³ However, we have used only solution measurements so far, and it would be advantageous to visualize what is occurring on an individual particle basis, as we show with transmission electron microscopy (TEM).

To examine what happens at the AgNP surface, we sought to capture the dissolution process using TEM (Figure 7). AgNPs (~50 to 80 nm) deposited onto TEM substrates were either fully dense spheres or spheres with surface defects that seem to be expelling silver. The images can be seen in Figure 7. Silver discharge from the core was observed several times on multiple substrates. However, BSA-AgNPs deposited onto TEM grids in the absence of HNO_3 never exhibited this phenomenon. Only upon acid treatment was a rupture in the surface observed.

We attribute this behavior to the localized disruption of the BSA corona and subsequent oxidative dissolution of the accessible AgNP surface. It is interesting that BSA coating

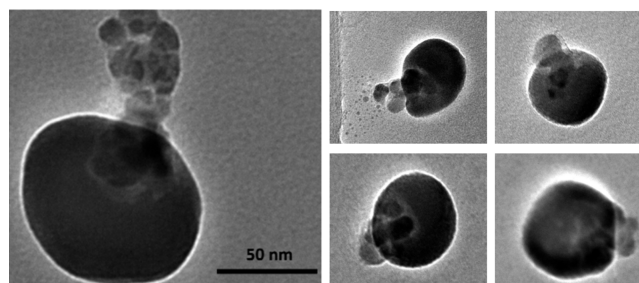


Figure 7. TEM images of larger BSA-AgNPs deposited on functionalized grids after 15 min of exposure to dilute nitric acid (i.e., 50 mM). Electrostatic anchoring to the grid minimizes sample-preparation-induced agglomeration. The local nature of the surface destabilization suggests that individual BSA molecules or small BSA bunches cannot provide stability to the Ag core, and silver leaks out of the compromised BSA-AgNP. This was never observed by TEM in particles not treated with acid. Once the BSA coating is breached, individual BSA-AgNPs will dissolve, as was observed under the electron beam (Supporting Information Movie S1). The 50 nm scale bar corresponds to all five different particles.

disruption is not uniform, but occurs at a local spot. We present two possibilities for the observed rupturing. First, BSA might not form a uniform protective coating around the entire particle, thus leaving spots on the surface vulnerable to acid attack (infiltration). Second, it is possible that BSA unfolds locally at a point on the AgNP surface where a nearby acidic concentration gradient exists in the solution medium, exposing the surface in the process (fluctuation). Regardless of the specific mechanism, it is clear that nitric acid causes acute and local disruption of the protein surface, leading to the dissolution of Ag from the particle core into the surrounding environment. Once the coating is breached, individual AgNPs are observed to dissolve very quickly.

Mechanism of BSA-AgNP Dissolution. To develop a working model of what is happening in the dissolving BSA-AgNP system, we bring together key results obtained from the USAXS measurements, application of the rate equations, and TEM. First, the principal population AgNP diameter does not change significantly during dissolution, whether particles agglomerate or stay singly dispersed. Second, the AgNP volume fraction decay during dissolution best fits a second-order rate equation when in a strong acid dissolution environment (i.e., once the BSA layer is breached). Third, by further interpreting the rate reaction analysis in Figure 6, we can infer that once the BSA coating is degraded by the nitric acid, AgNP loss is dominated by the oxidative dissolution of AgNPs into ions. Fourth, our TEM snapshots of the dissolution process for similar AgNPs reveal that acid-mediated surface destabilization results in plumes of high electron contrast silver (most likely oxide, sulfide, or chloride) erupting from the AgNPs and their subsequent rapid elimination.

All of these key results lead us to a model that is shown in the cartoon schematic in Figure 8. We postulate that a BSA corona can protect AgNPs well under harsh acid conditions (up to 250 mM), but once the BSA protein coating is breached, the NPs dissolve very quickly. This can happen due to statistical fluctuations in acid concentrations near a NP surface or by incomplete surface coverage of adsorbed BSA. A single compromised particle then dissolves rapidly because one 10-nm-diameter particle contains $\sim 10^{-19}$ mol Ag which interacts⁵⁴ with a ≥ 50 mM HNO_3 solution. The total measured AgNP

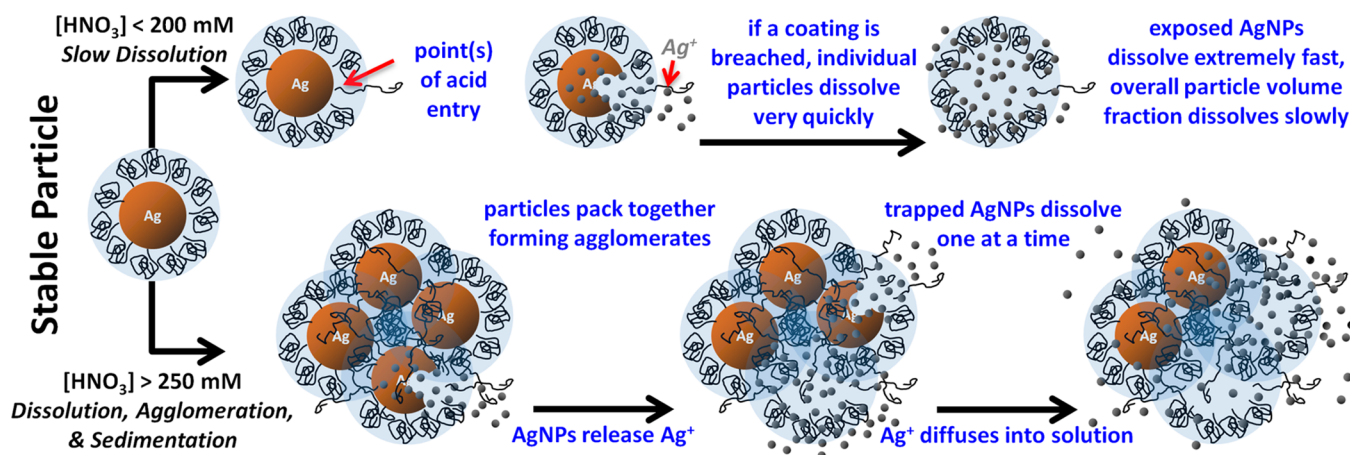


Figure 8. Working model of the colloidal destabilization, morphological transformations, and dissolution of BSA-protected AgNPs due to nitric acid. At low acid concentrations, BSA can stabilize particles, although nonuniformity in coatings or random acid attack can disrupt localized points on the particle surface, initiating dissolution. At high acid concentrations, the BSA corona destabilizes and particles cluster together, forming agglomerates. Silver will also dissolve from these agglomerates over time (whether sedimented or not).

volume fraction in the dissolving AgNP suspension is initially $\sim 2.5 \times 10^{-5}$, which equates to a 2.43 mM Ag solution (further calculations in the Supporting Information). This confirms that BSA has an enormous protecting effect on the particle surface because we observe such robust stabilization of 2.43 mM Ag (in NP form) in 50 mM HNO_3 .

If the concentration of acid added is above 250 mM HNO_3 , then the BSA protein coating is disrupted immediately, and particles agglomerate and sediment. However, by stirring the samples we were able to avoid the dominant effect of sedimentation. We infer that the NPs are still dissolved as individual entities, even though trapped in large BSA agglomerates. Thus, we can separate dissolution, agglomeration, and sedimentation to determine the release of Ag from dissolving NP systems. The processes compete, but BSA confers specific stability to the NP surface, which, once lost, causes the particle to disappear, much like popping bubbles as opposed to peeling back the layers of an onion.

CONCLUSIONS

We have quantified the dissolution, agglomeration, and stability limits of silver nanoparticles coated by a highly protective and ubiquitous protein: bovine serum albumin. By modeling the agglomerate morphology as packed spheres, we are able to extract from USAXS data the total amount of Ag released from NP form, and the kinetics of dissolution and agglomeration can be temporally examined and deconvoluted. Exploring BSA near its stability limits revealed three regimes. At the lowest nitric acid concentrations ($< 200 \text{ mM}$), the protein corona protected the particles from dissolution very well with negligible agglomeration. At medium acid levels ($< 250 \text{ mM}$), particles began to dissolve and agglomerate simultaneously. At the highest acid concentrations ($> 250 \text{ mM}$), the protein corona was destabilized and particles rapidly coagulated, forming large, eventually fractal, agglomerates. Because the dissolution and agglomeration processes compete, it is critical to separate their effects in situ in order to determine what happens overall in solution. AgNPs dissolve rapidly when the BSA coating is breached, whether the particles are individually dispersed or trapped in agglomerates. This results in a second-order reaction rate with respect to the disappearance of AgNPs which will

then release silver ions (Ag^+) as a consequence of oxidative dissolution.

Surface coatings are critical for protecting the surface of a reactive metal NP in solution, yet the stability limits of coating breakdown are often overlooked when examining NP reactions in mild or harsh environments. However, it is important to understand the mechanisms and conditions under which a protective coating fails because surface coatings play such essential roles in environmental health and safety studies of NPs. Coagulation of particles (agglomeration) and reactive metal ion release (dissolution), which is a potential environmental pollutant, are the two most basic fates for Ag in natural systems. Controlling the surface coating and measuring the total reaction environment is vital to understanding the basic mechanisms of AgNP transformation in solution. Chemical reactions of NPs in solution are specifically determined by the colloidal stability of reacting species, and the limiting factor in the colloidal destabilization (e.g., AgNP transformation²⁸ into Ag^+ and agglomerates) of NPs is the disruption of stable coating molecules and hence the roadblock to understanding NP–environment interactions. Both processes, agglomeration and dissolution, compete to remove individually dispersed particles from solution, which we have directly quantified in relation to the coating molecule's stability regimes. This method can be extended to other useful coatings and other metal NP systems in order to determine the fate and transformations of nanomaterials in environmentally relevant media or biological systems.

For example, previous work using other highly relevant coatings (e.g., citrate and polyvinylpyrrolidone (PVP)) highlighted the fact that cysteine, the constituent of BSA that binds to Ag, affects dissolution, agglomeration, and surface chemistry.⁵⁵ We found, as the authors predicted, that protein had a striking effect, drastically impacting AgNP dissolution kinetics and intermediate agglomerate morphologies formed during the destabilization process. Future work will look at the mechanistic breakdown of other biologically useful coatings such as citrate and PVP in order to determine their stabilizing potential toward reactive metal nanoparticles.

METHODS

Materials. The following chemicals were used as received⁵⁶ without further purification: AgNO₃, sodium citrate, NaBH₄ granules from Sigma-Aldrich (St. Louis, MO), 1.0 N HNO₃ from Titristar/Millipore (Billerica, MA), and bovine serum albumin crystals/powder from Seracare Life Sciences (Milford, MA). Particle-free deionized water was used to prepare all solutions.

Synthesis of Silver Nanoparticles, Quality Control, and TEM. Citrate and BSA-AgNPs were synthesized according to previous methods.^{24,57} Briefly, 3 L of water was brought to boiling in a glass beaker on a hot plate with a magnetic stir bar, to which 29.7 mL of a 58.9 mM solution of aqueous AgNO₃ was introduced. The solution was allowed to stir for 1 min, and then 5.11 mL of a 340 mM solution of aqueous sodium citrate was added. After 1 min of stirring, 20 mL of 100 mM NaBH₄ was added dropwise over 2 min under vigorous stirring. Then the solution was allowed to react for 30 min, upon which the beaker was removed from the hot plate to cool to room temperature. Particles were made for several USAXS experiments in this way and typically had Z_{ave} diameters of 17.6 ± 0.2 nm, with a polydispersity index (a DLS intensity-weighted polydispersity estimate) of 0.06 ± 0.02 , where uncertainties were calculated as the standard deviation of five measurements. DLS measurements were made with a Zetasizer Nano (Malvern Instruments, Westborough, MA) operating in 173° backscattering mode at 20.0 ± 0.1 °C, and UV-vis spectra were collected on a Lambda 750 spectrophotometer (PerkinElmer, Waltham, MA). In each case, disposable UV-transparent semimicro plastic cuvettes (Brandtech, Essex, CT) were used with a 1 mL sample volume. BSA (or other coatings, Supporting Information) was then added to the solution at 0.06 mg/mL and allowed to react, coating the particles.

Then particles were concentrated $\sim 10\times$ for USAXS measurements by N₂-pressurized stirred-cell ultrafiltration using 100 kDa regenerated cellulose membranes and a stirred cell apparatus (Millipore, Billerica, MA) at pressures of ~ 170 kPa (25 psi). DLS and UV-vis were employed at each step (after synthesis, after coating, and after concentration) to ensure quality control. No agglomerates or particle loss was detected. The 100 kDa cutoff allows free monomeric BSA (66 kDa) passage through the membrane, resulting in clear filtrate water with a soapy/foamy character, indicative of large quantities of excess free BSA. It should be noted that if the N₂ pressure was higher than ~ 240 kPa (35 psi), then BSA-AgNPs were observed to leak through the cellulose membrane, judging from a yellow AgNP color appearing in the filtrate. This is likely due to the compressibility of the soft-matter BSA coating or damage to the cellulose membrane structure. No centrifugation was performed because, as we have seen before,⁴³ significant particle loss can occur, and it is crucial for USAXS to have optimal concentrations, especially because we are losing material during the dissolution experiments. The resultant aqueous dispersions (prior to USAXS measurements) contain 4.86 mM Ag and significantly less than 9.02 μM BSA (bound + free) (further calculations in the Supporting Information). This 9.02 μM BSA concentration, before concentration/purification, was chosen to ensure a maximal coating density on the NP surface, based on measurements of larger AuNPs.⁴³

TEM was performed on a JEOL JEM3010 operating at 300 kV using amine-functionalized SiO₂ TEM grids (Dune Sciences, Eugene, OR). Briefly, larger BSA-AgNPs (~ 50 to 80 nm) were synthesized identically to the 10 nm particles. The only change in the synthesis was using one-tenth the amount of sodium citrate. This reduction in citrate allows the particles to grow larger because there is insufficient citrate to stabilize the total NP surface area. After being coated with BSA, dilute BSA-AgNPs were mixed with HNO₃, and the 50 mM solution allowed to process for 2 h. Then 40 μL of the dissolving sample was drop-cast on an amine-functionalized grid and allowed to react for 15 min. Excess NP solution was wicked away, and the grids were dried in a desiccator.

USAXS Measurement and Modeling. USAXS measurements were carried out at sector 15ID-D at the Advanced Photon Source (APS), Argonne National Laboratory.⁵⁸ The use of a flow-cell system

enabled a continuous flow of sample and acid, enabling in situ measurement, as described previously.⁵⁹ Briefly, 10 mL of the aqueous AgNPs were mixed with 10 mL of the nitric acid solutions and allowed to flow for one cycle before measurement began, during which monochromatic X-rays with energy 16.9 keV ($\lambda = 0.073$ nm) were used. The scattering data were corrected for parasitic background scattering and for attenuation (using data from an aqueous buffer). USAXS data, which are inherently slit-smear perpendicular to the scanning direction, were absolute calibrated with respect to the incident beam intensity according to first-principles methods. Data reduction, desmearing, and modeling were performed within the Indra 2 and Irena 2 packages of data evaluation and modeling macros⁶⁰ for Igor Pro (Wavemetrics, Lake Oswego, OR).

All parameters were modeled using standard least-squares fitting routines. Uncertainties in modeled parameters from USAXS measurements (i.e., volume fraction) were estimated to be $\pm 5\%$ standard deviations on each data point. For calculated values using these measurements, the propagation of uncertainties was undertaken by the method of partial derivatives.

ASSOCIATED CONTENT

Supporting Information

DLS and UV-vis plots demonstrating the stability of the synthesized particles, calculations for NP dissolution, discussion of fine cluster particles, sedimentation profiles for nonstirred dissolution, fractal analyses, USAXS plots from representative samples, AgNP size distributions, a movie showing a single dissolving BSA-AgNP, background theory on dense particle packing, and calculations on internal agglomerate structure. This material is available free of charge via the Internet at <http://pubs.acs.org>.

AUTHOR INFORMATION

Corresponding Author

*E-mail: matthew.n.martin@gmail.com.

Author Contributions

The manuscript was written through the contributions of all authors. All authors have given approval to the final version of the manuscript.

Notes

The authors declare no competing financial interest.

ACKNOWLEDGMENTS

M.N.M. thanks J. Pettibone, F. Zhang, and D. Wang for many helpful discussions and for manuscript review as well. We are grateful to J. Ilavsky and J. Bonevich for invaluable assistance with USAXS and TEM measurements, respectively. M.N.M. acknowledges support under the NIST American Recovery and Reinvestment Act (NIST-ARRA) Measurement Science and Engineering Fellowship Program Award 70NANB10H026 through the University of Maryland. ChemMatCARS Sector 15 is principally supported by the Divisions of Chemistry (CHE) and Materials Research (DMR), National Science Foundation, under grant number NSF/CHE-1346572. Use of the Advanced Photon Source, an Office of Science User Facility operated for the U.S. Department of Energy (DOE) Office of Science by Argonne National Laboratory, was supported by the U.S. DOE under contract no. DE-AC02-06CH11357.

ABBREVIATIONS

BSA, bovine serum albumin; AgNP, silver nanoparticle; USAXS, ultra-small-angle X-ray scattering; UV-vis, ultra-violet-visible spectroscopy; DLS, dynamic light scattering

REFERENCES

- (1) Tolaymat, T. M.; El Badawy, A. M.; Genaidy, A.; Scheckel, K. G.; Luxton, T. P.; Suidan, M. An Evidence-Based Environmental Perspective of Manufactured Silver Nanoparticle in Syntheses and Applications: A Systematic Review and Critical Appraisal of Peer-Reviewed Scientific Papers. *Sci. Total Environ.* **2010**, *408*, 999–1006.
- (2) Ahamed, M.; AlSalhi, M. S.; Siddiqui, M. K. J. Silver Nanoparticle Applications and Human Health. *Clin. Chim. Acta* **2010**, *411*, 1841–1848.
- (3) Fabrega, J.; Luoma, S. N.; Tyler, C. R.; Galloway, T. S.; Lead, J. R. Silver Nanoparticles: Behaviour and Effects in the Aquatic Environment. *Environ. Int.* **2011**, *37*, 517–531.
- (4) Kittler, S.; Greulich, C.; Diendorf, J.; Köller, M.; Epple, M. Toxicity of Silver Nanoparticles Increases during Storage Because of Slow Dissolution under Release of Silver Ions. *Chem. Mater.* **2010**, *22*, 4548–4554.
- (5) Liu, J.; Hurt, R. H. Ion Release Kinetics and Particle Persistence in Aqueous Nano-Silver Colloids. *Environ. Sci. Technol.* **2010**, *44*, 2169–2175.
- (6) Dobias, J.; Bernier-Latmani, R. Silver Release from Silver Nanoparticles in Natural Waters. *Environ. Sci. Technol.* **2013**, *47*, 1410–1416.
- (7) Glover, R. D.; Miller, J. M.; Hutchison, J. E. Generation of Metal Nanoparticles from Silver and Copper Objects: Nanoparticle Dynamics on Surfaces and Potential Sources of Nanoparticles in the Environment. *ACS Nano* **2011**, *5*, 8950–8957.
- (8) Akaighe, N.; MacCuspie, R. I.; Navarro, D. A.; Aga, D. S.; Banerjee, S.; Sohn, M.; Sharma, V. K. Humic Acid-Induced Silver Nanoparticle Formation Under Environmentally Relevant Conditions. *Environ. Sci. Technol.* **2011**, *45*, 3895–3901.
- (9) Yin, Y.; Liu, J.; Jiang, G. Sunlight-Induced Reduction of Ionic Ag and Au to Metallic Nanoparticles by Dissolved Organic Matter. *ACS Nano* **2012**, *6*, 7910–7919.
- (10) AshaRani, P. V.; Low Kah Mun, G.; Hande, M. P.; Valiyaveetil, S. Cytotoxicity and Genotoxicity of Silver Nanoparticles in Human Cells. *ACS Nano* **2009**, *3*, 279–290.
- (11) Wijnhoven, S. W. P.; Peijnenburg, W. J. G. M.; Herberths, C. A.; Hagens, W. I.; Oomen, A. G.; Heugens, E. H. W.; Roszek, B.; Bisschops, J.; Gosens, I.; Van De Meent, D.; et al. Nano-Silver – a Review of Available Data and Knowledge Gaps in Human and Environmental Risk Assessment. *Nanotoxicology* **2009**, *3*, 109–138.
- (12) Chen, J.; Han, C.; Lin, X.; Tang, Z.; Su, S. Effect of Silver Nanoparticle Dressing on Second Degree Burn Wound. *Zhonghua Wai Ke Za Zhi* **2006**, *44*, 50–52.
- (13) Liu, J.; Sonshine, D. A.; Shervani, S.; Hurt, R. H. Controlled Release of Biologically Active Silver from Nanosilver Surfaces. *ACS Nano* **2010**, *4*, 6903–6913.
- (14) Li, X.; Lenhart, J. J.; Walker, H. W. Dissolution-Accompanied Aggregation Kinetics of Silver Nanoparticles. *Langmuir* **2010**, *26*, 16690–16698.
- (15) Li, L.; Zhu, Y.-J. High Chemical Reactivity of Silver Nanoparticles toward Hydrochloric Acid. *J. Colloid Interface Sci.* **2006**, *303*, 415–418.
- (16) Rogers, K. R.; Bradham, K.; Tolaymat, T.; Thomas, D. J.; Hartmann, T.; Ma, L.; Williams, A. Alterations in Physical State of Silver Nanoparticles Exposed to Synthetic Human Stomach Fluid. *Sci. Total Environ.* **2012**, *420*, 334–339.
- (17) Dominguez-Medina, S.; Blankenburg, J.; Olson, J.; Landes, C. F.; Link, S. Adsorption of a Protein Monolayer via Hydrophobic Interactions Prevents Nanoparticle Aggregation under Harsh Environmental Conditions. *ACS Sustainable Chem. Eng.* **2013**, *1*, 833–842.
- (18) Levard, C.; Hotze, E. M.; Lowry, G. V.; Brown, G. E. Environmental Transformations of Silver Nanoparticles: Impact on Stability and Toxicity. *Environ. Sci. Technol.* **2012**, *46*, 6900–6914.
- (19) Levard, C.; Reinsch, B. C.; Michel, F. M.; Oumahi, C.; Lowry, G. V.; Brown, G. E. Sulfidation Processes of PVP-Coated Silver Nanoparticles in Aqueous Solution: Impact on Dissolution Rate. *Environ. Sci. Technol.* **2011**, *45*, 5260–5266.
- (20) Elzey, S.; Grassian, V. Agglomeration, Isolation and Dissolution of Commercially Manufactured Silver Nanoparticles in Aqueous Environments. *J. Nanopart. Res.* **2010**, *12*, 1945–1958.
- (21) Li, X.; Lenhart, J. J. Aggregation and Dissolution of Silver Nanoparticles in Natural Surface Water. *Environ. Sci. Technol.* **2012**, *46*, 5378–5386.
- (22) Consumer Products Inventory, Project for Emerging Nanotechnologies, Woodrow Wilson International Center for Scholars; <http://www.nanotechproject.org/inventories/consumer/>, accessed August, 2012.
- (23) Kennedy, A. J.; Hull, M. S.; Bednar, A. J.; Goss, J. D.; Gunter, J. C.; Bouldin, J. L.; Vikesland, P. J.; Steevens, J. A. Fractionating Nanosilver: Importance for Determining Toxicity to Aquatic Test Organisms. *Environ. Sci. Technol.* **2010**, *44*, 9571–9577.
- (24) Zook, J.; Long, S.; Cleveland, D.; Geronimo, C.; MacCuspie, R. Measuring Silver Nanoparticle Dissolution in Complex Biological and Environmental Matrices Using UV–Visible Absorbance. *Anal. Bioanal. Chem.* **2011**, *401*, 1993–2002.
- (25) Tsai, D.-H.; Cho, T. J.; DelRio, F. W.; Taurozzi, J.; Zachariah, M. R.; Hackley, V. A. Hydrodynamic Fractionation of Finite Size Gold Nanoparticle Clusters. *J. Am. Chem. Soc.* **2011**, *133*, 8884–8887.
- (26) Zook, J. M.; Rastogi, V.; MacCuspie, R. I.; Keene, A. M.; Fagan, J. Measuring Agglomerate Size Distribution and Dependence of Localized Surface Plasmon Resonance Absorbance on Gold Nanoparticle Agglomerate Size Using Analytical Ultracentrifugation. *ACS Nano* **2011**, *5*, 8070–8079.
- (27) Tiede, K.; Boxall, A. B. A.; Tiede, D.; Tear, S. P.; David, H.; Lewis, J. A Robust Size-Characterisation Methodology for Studying Nanoparticle Behaviour in “Real” Environmental Samples, Using Hydrodynamic Chromatography Coupled to ICP-MS. *J. Anal. At. Spectrom.* **2009**, *24*, 964–972.
- (28) Pettibone, J. M.; Gigault, J.; Hackley, V. A. Discriminating the States of Matter in Metallic Nanoparticle Transformations: What Are We Missing? *ACS Nano* **2013**, *7*, 2491–2499.
- (29) Baalousha, M.; Lead, J. R. Rationalizing Nanomaterial Sizes Measured by Atomic Force Microscopy, Flow Field-Flow Fractionation, and Dynamic Light Scattering: Sample Preparation, Polydispersity, and Particle Structure. *Environ. Sci. Technol.* **2012**, *46*, 6134–6142.
- (30) Li, X.; Lenhart, J. J.; Walker, H. W. Aggregation Kinetics and Dissolution of Coated Silver Nanoparticles. *Langmuir* **2012**, *28*, 1095–1104.
- (31) Huynh, K. A.; Chen, K. L. Aggregation Kinetics of Citrate and Polyvinylpyrrolidone Coated Silver Nanoparticles in Monovalent and Divalent Electrolyte Solutions. *Environ. Sci. Technol.* **2011**, *45*, 5564–5571.
- (32) Brewer, S. H.; Glomm, W. R.; Johnson, M. C.; Knag, M. K.; Franzen, S. Probing BSA Binding to Citrate-Coated Gold Nanoparticles and Surfaces. *Langmuir* **2005**, *21*, 9303–9307.
- (33) Rezwani, K.; Studart, A. R.; Vörös, J.; Gauckler, L. J. Change of ζ Potential of Biocompatible Colloidal Oxide Particles upon Adsorption of Bovine Serum Albumin and Lysozyme. *J. Phys. Chem. B* **2005**, *109*, 14469–14474.
- (34) Casals, E.; Pfaller, T.; Duschl, A.; Oostingh, G. J.; Püntes, V. Time Evolution of the Nanoparticle Protein Corona. *ACS Nano* **2010**, *4*, 3623–3632.
- (35) Dominguez-Medina, S.; McDonough, S.; Swanglap, P.; Landes, C. F.; Link, S. In Situ Measurement of Bovine Serum Albumin Interaction with Gold Nanospheres. *Langmuir* **2012**, *28*, 9131–9139.
- (36) Tanford, C.; Buzzell, J. G. The Viscosity of Aqueous Solutions of Bovine Serum Albumin between pH 4.3 and 10.5. *J. Phys. Chem.* **1956**, *60*, 225–231.
- (37) Tanford, C.; Swanson, S. A.; Shore, W. S. Hydrogen Ion Equilibria of Bovine Serum Albumin. *J. Am. Chem. Soc.* **1955**, *77*, 6414–6421.
- (38) Nicolosi, V.; Vrbancic, D.; Mrzel, A.; McCauley, J.; O’Flaherty, S.; McGuinness, C.; Compagnini, G.; Mihailovic, D.; Blau, W. J.; Coleman, J. N. Solubility of $\text{Mo}_6\text{S}_4\text{I}_{4.5}$ Nanowires in Common Solvents: A Sedimentation Study. *J. Phys. Chem. B* **2005**, *109*, 7124–7133.

- (39) Royall, C. P.; Roij, R. van; Blaaderen, A. van. Extended Sedimentation Profiles in Charged Colloids: The Gravitational Length, Entropy, and Electrostatics. *J. Phys.: Condens. Matter* **2005**, *17*, 2315–2326.
- (40) Phenrat, T.; Saleh, N.; Sirk, K.; Tilton, R. D.; Lowry, G. V. Aggregation and Sedimentation of Aqueous Nanoscale Zerovalent Iron Dispersions. *Environ. Sci. Technol.* **2007**, *41*, 284–290.
- (41) Peters, T. *All About Albumin*; Academic Press: San Diego, 1995.
- (42) Barbosa, L. R. S.; Ortore, M. G.; Spinozzi, F.; Mariani, P.; Bernstorff, S.; Itri, R. The Importance of Protein-Protein Interactions on the pH-Induced Conformational Changes of Bovine Serum Albumin: A Small-Angle X-ray Scattering Study. *Biophys. J.* **2010**, *98*, 147–157.
- (43) Tsai, D.-H.; DelRio, F. W.; Keene, A. M.; Tyner, K. M.; MacCuspie, R. I.; Cho, T. J.; Zachariah, M. R.; Hackley, V. A. Adsorption and Conformation of Serum Albumin Protein on Gold Nanoparticles Investigated Using Dimensional Measurements and in Situ Spectroscopic Methods. *Langmuir* **2011**, *27*, 2464–2477.
- (44) Carter, D. C.; Ho, J. X. Structure of Serum Albumin. In *Lipoproteins, Apolipoproteins, and Lipases*; Schumaker, V. N., Ed.; Advances in Protein Chemistry; Academic Press: San Diego, 1994; Vol. 45, pp 153–203.
- (45) Beaucage, G.; Ulibarri, T. A.; Black, E. P.; Schaefer, D. W. Multiple Size Scale Structures in Silica—Siloxane Composites Studied by Small-Angle Scattering. In *Hybrid Organic-Inorganic Composites*; ACS Symposium Series; American Chemical Society: Washington, DC, 1995; Vol. 585, pp 97–111.
- (46) Hales, T. C.; Ferguson, S. P. A Formulation of the Kepler Conjecture. *Discrete Comput. Geom.* **2006**, *36*, 21–69.
- (47) Song, C.; Wang, P.; Makse, H. A. A Phase Diagram for Jammed Matter. *Nature* **2008**, *453*, 629–632.
- (48) Jaeger, H. M.; Nagel, S. R. Physics of the Granular State. *Science* **1992**, *255*, 1523–1531.
- (49) Valverde, J. M.; Castellanos, A. Random Loose Packing of Cohesive Granular Materials. *Europhys. Lett.* **2006**, *75*, 985–991.
- (50) Torquato, S.; Truskett, T. M.; Debenedetti, P. G. Is Random Close Packing of Spheres Well Defined? *Phys. Rev. Lett.* **2000**, *84*, 2064–2067.
- (51) Schaefer, D. W.; Martin, J. E.; Wiltzius, P.; Cannell, D. S. Fractal Geometry of Colloidal Aggregates. *Phys. Rev. Lett.* **1984**, *52*, 2371–2375.
- (52) Nam, C. H.; Pfeffer, R.; Dave, R. N.; Sundaresan, S. Aerated Vibrofluidization of Silica Nanoparticles. *AIChE J.* **2004**, *50*, 1776–1785.
- (53) We found that aqueous BSA-AgNPs were stable for over 1 year at room temperature, whereas citrate-AgNPs dissolved back into metallic silver within several months (data omitted). It should be noted that citrate can stabilize nonoxidizing metal nanoparticles, such as gold, for years. Thus in environments composed of nitric acid and dissolved oxygen, it is understandable that BSA-AgNPs exhibit different stability thresholds against oxidative dissolution completely based on the stability thresholds of BSA itself.
- (54) Tatarchuk, V. V.; Bulavchenko, A. I.; Druzhinina, I. A. Dissolution Kinetics of Silver Metal Nanoparticles in Their Reaction with Nitric Acid in an Reverse Micelle Solution of AOT. *Russ. J. Inorg. Chem.* **2007**, *52*, 1284–1288.
- (55) Gondikas, A. P.; Morris, A.; Reinsch, B. C.; Marinakos, S. M.; Lowry, G. V.; Hsu-Kim, H. Cysteine-Induced Modifications of Zero-Valent Silver Nanomaterials: Implications for Particle Surface Chemistry, Aggregation, Dissolution, and Silver Speciation. *Environ. Sci. Technol.* **2012**, *46*, 7037–7045.
- (56) The identification of any commercial product or trade name does not imply endorsement or recommendation by the National Institute of Standards and Technology.
- (57) MacCuspie, R. I.; Allen, A. J.; Hackley, V. A. Dispersion Stabilization of Silver Nanoparticles in Synthetic Lung Fluid Studied under In Situ Conditions. *Nanotoxicology* **2011**, *5*, 140–156.
- (58) Ilavsky, J.; Jemian, P. R.; Allen, A. J.; Zhang, F.; Levine, L. E.; Long, G. G. Ultra-Small-Angle X-ray Scattering at the Advanced Photon Source. *J. Appl. Crystallogr.* **2009**, *42*, 469–479.
- (59) Allen, A. J.; Hackley, V. A.; Jemian, P. R.; Ilavsky, J.; Raitano, J. M.; Chan, S.-W. In Situ Ultra-Small-Angle X-ray Scattering Study of the Solution-Mediated Formation and Growth of Nanocrystalline Ceria. *J. Appl. Crystallogr.* **2008**, *41*, 918–929.
- (60) Ilavsky, J.; Jemian, P. R. Irena: Tool Suite for Modeling and Analysis of Small-Angle Scattering. *J. Appl. Crystallogr.* **2009**, *42*, 347–353.